

# ARIA: ON THE INTERACTION BETWEEN ARCHITECTURES, AGGREGATION METHODS AND INITIALIZATIONS IN FEDERATED VISUAL CLASSIFICATION

Vasilis Siomos<sup>1</sup>, Sergio Naval-Marimont<sup>1</sup>, Jonathan Passerat-Palmbach<sup>1,2</sup>, Giacomo Tarroni<sup>1,2</sup>

<sup>1</sup> CitAI Research Centre, Department of Computer Science City, University of London

<sup>2</sup> BioMedIA, Department of Computing, Imperial College London

## ABSTRACT

Federated Learning (FL) is a collaborative training paradigm that allows for privacy-preserving learning of cross-institutional models by eliminating the exchange of sensitive data and instead relying on the exchange of model parameters between the clients and a server. Despite individual studies on how client models are aggregated, and, more recently, on the benefits of ImageNet pre-training, there is a lack of understanding of the effect the architecture chosen for the federation has, and of how the aforementioned elements interconnect. To this end, we conduct the first joint ARchitecture-Initialization-Aggregation study and benchmark ARIAs across a range of medical image classification tasks. We find that, contrary to current practices, ARIA elements have to be chosen together to achieve the best possible performance. Our results also shed light on good choices for each element depending on the task, the effect of normalisation layers, and the utility of SSL pre-training, pointing to potential directions for designing FL-specific architectures and training pipelines.

**Index Terms**— Federated Learning, Self-Supervised Pre-training

## 1. INTRODUCTION

Federated learning (FL) for healthcare [1] has emerged as a promising approach that enables collaborative machine learning without direct access to raw patient data. The typical scenario for medical imaging data is the cross-silo setting, where a small number of data owners/stakeholders fully participate in a round of federated training by training their local/client models and sending the parameters to a central server, which aggregates the client models into a server/global model. The global model is then broadcasted to all clients to start the next round, until training stops, and the final model is delivered to the stakeholders for deployment.

Since the seminal FedAvg paper [2], progress in cross-silo visual classification has been hard to determine, with innovation often focusing on improving the aggregation strategy for the frequent scenario where the client datasets are heterogeneous [3, 4]. Unfortunately, proposed methods most commonly use randomly initialized model weights, small/toy models, or both [5]. This makes comparing and drawing conclusions for real-world medical settings difficult.

Recent studies [6, 7] have been exploring the value of using ImageNet (IN) pre-trained networks for FL, showcasing improvements in closing the gap to centralised performance, improving overall performance, and reducing the effect of data heterogeneity. Another study by Qu et al. [8] highlighted the benefits of using IN pre-trained transformers for FL. Very recently, Pieri et al. [5] focused on the interaction of aggregation methods and architectures, but only examined IN pre-trained weights.

It’s important to note IN pre-training restricts the input to 224x224 RGB images. When up-sampling of the original images is required to achieve that, it leads to a bigger than necessary computational and memory load, and the introduction of aliasing artifacts (e.g. Fig. 1). When down-sampling is required instead, it can degrade performance. Hence, IN pre-training is not a silver bullet, and benchmarking architectures and aggregation strategies without pre-training is also important. Furthermore, task-relevant pre-training through self-supervised learning (SSL) has recently emerged as a highly-effective alternative to IN pre-training [9], but its usefulness in the FL setting remains largely unexplored.

Motivated by the above, we conduct what, to the best of our knowledge, is the first study to jointly examine ARIAs: Architecture-Initialization-Aggregation combinations: we select 9 architectures, with the weights initialized from 3 starting points (Random, ImageNet, SSL on a relevant dataset), and use 3 of the most common methods (FedAvg, FedOpt, SCAFFOLD) to aggregate the models. We focus on perhaps the most beneficial domain for FL, medical imaging, and evaluate the resulting ARIAs on 3 different medical imaging datasets, namely Fed-ISIC, and two versions of OrganAM-NIST (with and without simulated heterogeneity).

Our results after training more than 300 ARIAs indicate to researchers and practitioners designing FL pipelines for medical imaging data that all elements of an ARIA have to be evaluated together, but also shed light on the individual effects of network size, normalization methods, architecture choice, and utility of SSL pre-training.

## 2. METHODS

### 2.1. (AR)chitectures

We base our model choices around comparing popular architectures from the convolutional and transformer families, while also trying to pinpoint specific characteristics that help FL training, rather than restricting our choices based on model size or speed. To allow readers to compare, we include model parameter count in this section, and IN top-1 accuracy and measured training throughput in Tables 1,2,3.

Due to the ubiquity of residual networks [10], we choose a ResNet-18 (11.7M parameters), a ResNet-50 (25.6M), and a Wide-ResNet-50-2 [11] (68.9M), to examine the effect of residual depth and width. We add to those a DenseNet-121 [12] (8M), where every layer is connected to all others, to examine how the density of residual connections and feature re-use affect performance.

It bears noting these architectures employ Batch Normalisation (BN), which is known to degrade FL performance in heterogeneous settings [13]. To provide insight into alternatives to BN, we add a Normalization-Free (NF) ResNet-50 [14] (25.6M) to our list. NF architectures rely on so-called Scaled Weight Standardization (SWS),

**Table 1.** Average balanced accuracy across 6 clients on Fed-ISIC. IN top-1 accuracy reported next to model name. Models listed in decreasing measured training throughput (using AMP). Difference from average balanced accuracy of centrally trained model in parentheses.

Initialization	Random			ImageNet Pre-Training			DINO on Skin SSL dataset		
Agg. Method	FedAvg	FedOpt	SCAFFOLD	FedAvg	FedOpt	SCAFFOLD	FedAvg	FedOpt	SCAFFOLD
ResNet-18 (69.76)	51.65 (↓ 9.8)	46.7 (↓ 14.7)	52.45 (↓ 9)	65.87 (↓ 4.3)	67.55 (↓ 2.6)	68.66 (↓ 1.5)	66.57 (↓ 5.7)	62.36 (↓ 10)	66.87 (↓ 5.4)
NF-ResNet-50 (80.64)	55.93 (↓ 6.1)	56.25 (↓ 5.8)	<b>59.64 (↓ 2.4)</b>	71.88 (↑ 0.9)	68.75 (↓ 2.2)	71.53 (↑ 0.5)	67.83 (↓ 0.7)	67.92 (↓ 0.6)	70.11 (↑ 1.6)
ResNet-50 (80.86)	49.11 (↓ 12)	46.91 (↓ 14.2)	48.13 (↓ 13)	67.97 (↓ 6.3)	66.16 (↓ 8.1)	68.48 (↓ 5.8)	65.16 (↓ 7.2)	66.46 (↓ 5.9)	66.34 (↓ 6)
WRN-50-2 (81.6)	50.53 (↓ 8)	50.12 (↓ 8.4)	51.03 (↓ 7.5)	69.54 (↓ 5.3)	67.68 (↓ 7.2)	70.34 (↓ 4.5)	65.56 (↓ 6.9)	64.22 (↓ 8.3)	66.66 (↓ 5.8)
DenseNet-121 (74.43)	49.42 (↓ 13.3)	45.95 (↓ 16.8)	52.79 (↓ 9.9)	67.34 (↓ 5.8)	68.03 (↓ 5)	68.52 (↓ 4.6)	66.28 (↓ 5.3)	64.94 (↓ 6.6)	67.38 (↓ 4.2)
SWIN-T (81.47)	45.73 (↑ 23.2)	44.13 (↑ 21.6)	45.00 (↑ 22.5)	71.19 (↓ 1.3)	71.81 (↓ 0.6)	73.13 (↑ 0.7)	72.13 (↑ 1.7)	71.40 (↑ 0.9)	73.77 (↑ 3.3)
EfficientNetV2-S (84.22)	46.59 (↓ 10.8)	46.59 (↓ 10.8)	47.51 (↓ 9.8)	70.00 (↓ 9.6)	71.48 (↓ 8.1)	73.18 (↓ 6.4)	57.99 (↓ 14.9)	59.74 (↓ 13.1)	64.98 (↓ 7.9)
ViT-B-16 (81.07)	47.84 (↑ 7.2)	49.52 (↑ 8.9)	48.44 (↑ 7.8)	65.86 (↑ 1.6)	65.18 (↑ 0.9)	68.09 (↓ 3.8)	71.06 (↓ 2.9)	71.52 (↓ 2.5)	69.49 (↓ 4.5)
ConvNext-S (83.61)	48.10 (↓ 7.9)	49.93 (↓ 6.1)	48.56 (↓ 7.5)	<b>75.08 (↓ 0.1)</b>	73.40 (↓ 1.7)	74.28 (↓ 0.8)	72.07 (↓ 3)	73.57 (↓ 1.5)	<b>74.56 (↓ 0.5)</b>

**Table 2.** Average accuracy across 4 clients on OrganAMNIST with  $\alpha = 0.1$ . IN top-1 accuracy reported next to model name. Models listed in decreasing measured training throughput (using AMP). Difference from accuracy of centrally trained model in parentheses.

Initialization	Random			ImageNet Pre-Training			DINO on Abdomen-SSL		
Agg. Method	FedAvg	FedOpt	SCAFFOLD	FedAvg	FedOpt	SCAFFOLD	FedAvg	FedOpt	SCAFFOLD
ResNet-18 (69.76)	88.8 (↓5.6)	90.76 (↓3.6)	89.16 (↓5.2)	94.02 (↓1.9)	94.78 (↓1.2)	94.33 (↓1.6)	83.54 (↓9.8)	87.89 (↓5.5)	84.76 (↓8.6)
NF-ResNet-50 (80.64)	71.6 (↓16.3)	78.84 (↓9.1)	73.8 (↓14.1)	94.39 (↓1.4)	95.26 (↓0.5)	95.2 (↓0.6)	84.58 (↓7.9)	87.93 (↓4.5)	86.92 (↓5.5)
ResNet-50 (80.86)	83.32 (↓10.5)	86.6 (↓7.2)	84.82 (↓9.0)	91.98 (↓3.5)	92.98 (↓2.5)	92.32 (↓3.1)	81.33 (↓12.9)	85.69 (↓8.5)	81.49 (↓12.8)
WRN-50-2 (81.6)	84.52 (↓9.6)	85.58 (↓8.5)	83.82 (↓10.3)	90.56 (↓4.3)	91.71 (↓3.2)	90.4 (↓4.5)	79.98 (↓13.7)	85.02 (↓8.6)	77.09 (↓16.5)
DenseNet-121 (74.43)	86.01 (↓8.6)	89.12 (↓5.5)	85.06 (↓9.6)	94.72 (↓2.2)	95.1 (↓1.9)	94.68 (↓2.3)	85.26 (↓9.2)	89.21 (↓5.3)	84.94 (↓9.5)
SWIN-T (81.474)	83.03 (↓8.6)	85.17 (↓6.4)	83.16 (↓8.4)	95.64 (↓0.6)	95.83 (↓0.4)	95.83 (↓0.4)	83.4 (↓8.2)	86.4 (↓5.2)	84.8 (↓6.8)
EfficientNetV2-S (84.22)	88.8 (↓6.2)	<b>91.46 (↓3.6)</b>	89.19 (↓5.9)	94.0 (↓2.7)	94.26 (↓2.4)	93.46 (↓3.2)	61.19 (↓31.6)	67.54 (↓25.3)	56.2 (↓36.6)
ViT-B-16 (81.072)	83.14 (↓4.2)	83.52 (↓3.9)	83.85 (↓3.5)	95.3 (↓1.5)	95.96 (↓0.9)	<b>96.01 (↓0.8)</b>	81.34 (↓6.8)	83.76 (↓4.4)	81.99 (↓6.2)
ConvNext-S (83.61)	53.76 (↓35.4)	56.07 (↓33.1)	55.34 (↓33.8)	94.12 (↓2.6)	94.92 (↓1.8)	94.84 (↓1.9)	87.31 (↓6.0)	<b>89.68 (↓3.7)</b>	87.64 (↓5.7)

i.e. careful scaling of weights, instead of normalization, to achieve correct signal propagation during learning.

As for transformer architectures, we include a ViT-B-16 [15] (86.6M) and a SWIN-T [16] (28.3M), to compare convolution with self-attention. Both employ Layer Normalization (LN).

Since the emergence of vision transformers, more advanced convolutional architectures have been introduced with the goal of outperforming them, and we pick EfficientNetV2-S [17] (21.5M, uses BN), an evolution of ResNets guided by neural architecture search, and ConvNext-S [18] (50.2M, uses LN), which borrows design principles from SWIN transformers to modernize the typical convolutional network structure.

## 2.2. (I)Initialization

In medical imaging scenarios it is often the case that i) the target task images are dissimilar to natural ones, ii) there are similar medical datasets publicly available. Based on that observation, besides random initialization and IN pre-training, we construct two task-relevant pre-training datasets, Abdomen-SSL and Skin-SSL, respectively, and train the models using self-supervised learning (SSL) as a pre-cursor task using the DINO [19] algorithm, which is compatible with both transformers and convolutional networks, and relies on self-distillation. We pre-train for 100 epochs for Abdomen-SSL, and 300 for Skin-SSL, based on the loss decrease of DINO.

## 2.3. (A)Aggregation methods

To perform our study, we select three of the most common aggregation strategies, namely FedAvg, FedOpt, and SCAFFOLD.

**FedAvg** [2] is the simplest parameter averaging method, constructing the global model as the weighted average of client models.

**FedOpt** [20] is a framework describing the de-coupling of the server-side and client-side optimization, under which the server can

employ any optimizer like SGD, Adam, etc. We use SGD with momentum at the server, similar to FedAvgM [3], with the addition of a cosine scheduler to decrease the server learning rate as training progresses. The server learning rate was fixed to 1.0, chosen from {0.5, 1}, and the momentum to 0.6, chosen from {0.6, 0.9}.

**SCAFFOLD** [4] is an aggregation method utilizing control variates to correct local model updates against the so-called client-drift (divergence from the global model). While training throughput is mostly unaffected, it does require twice the bandwidth and memory due to the control variates being communicated and stored at each client.

## 3. EXPERIMENTS

### 3.1. Datasets

We conduct experiments on OrganAMNIST [21] and Fed-ISIC [22]. The latter is already federated, and for the former we construct a federated version of 4 clients, by utilizing the commonly-used Dirichlet partitioning strategy [3], which induces both dataset size and label distribution heterogeneity based on the controllable concentration parameter  $\alpha$ . We examine an IID setting by setting  $\alpha = 100$ , and a highly heterogeneous one by setting  $\alpha = 0.1$ . This leads to a sufficiently wide range of difficulty to benchmark the chosen models, from the grayscale IID OrganAMNIST to the highly imbalanced, both in label distribution and data size RGB, Fed-ISIC. Moreover, the distance between the domains and ImageNet provides more insight into learning dynamics for the medical community compared to testing on natural images.

**OrganAMNIST** [21] consists of 58,850 28x28 grayscale images across 11 organ labels segmented from axial slices of abdominal CT scans. We upscale the images to 224x224 and copy the channel over 3 times for compatibility with IN pre-trained models. Each

**Table 3.** Average accuracy across 4 clients on OrganAMNIST with  $\alpha = 100$ . IN top-1 accuracy reported next to model name. Models listed in decreasing measured training throughput (using AMP). Difference from accuracy of centrally trained model in parentheses.

Initialization	Random			ImageNet Pre-Training			DINO on Abdomen-SSL		
Agg. Method	FedAvg	FedOpt	SCAFFOLD	FedAvg	FedOpt	SCAFFOLD	FedAvg	FedOpt	SCAFFOLD
ResNet-18 (69.76)	93.8 ( $\downarrow 0.6$ )	94.3 ( $\downarrow 0.1$ )	93.97 ( $\downarrow 0.4$ )	96.05 ( $\uparrow 0.1$ )	96.38 ( $\uparrow 0.4$ )	95.99 ( $\downarrow 0.0$ )	92.06 ( $\downarrow 1.3$ )	93.47 ( $\uparrow 0.1$ )	92.14 ( $\downarrow 1.2$ )
NF-ResNet-50 (80.64)	84.28 ( $\downarrow 3.6$ )	88.09 ( $\uparrow 0.2$ )	84.4 ( $\downarrow 3.5$ )	95.5 ( $\downarrow 0.3$ )	95.64 ( $\downarrow 0.1$ )	95.6 ( $\downarrow 0.2$ )	92.08 ( $\downarrow 0.4$ )	92.74 ( $\uparrow 0.3$ )	92.09 ( $\downarrow 0.4$ )
ResNet-50 (80.86)	93.39 ( $\downarrow 0.5$ )	94.0 ( $\uparrow 0.2$ )	93.54 ( $\downarrow 0.3$ )	94.98 ( $\downarrow 0.5$ )	95.56 ( $\uparrow 0.1$ )	95.34 ( $\downarrow 0.1$ )	92.8 ( $\downarrow 1.4$ )	<b>93.51 (<math>\downarrow 0.7</math>)</b>	92.69 ( $\downarrow 1.5$ )
WRN-50-2 (81.6)	93.74 ( $\downarrow 0.3$ )	93.99 ( $\downarrow 0.1$ )	93.72 ( $\downarrow 0.4$ )	94.7 ( $\downarrow 0.2$ )	95.42 ( $\uparrow 0.5$ )	94.76 ( $\downarrow 0.1$ )	92.24 ( $\downarrow 1.4$ )	93.1 ( $\downarrow 0.5$ )	92.52 ( $\downarrow 1.1$ )
DenseNet-121 (74.43)	93.95 ( $\downarrow 0.7$ )	94.28 ( $\downarrow 0.3$ )	93.66 ( $\downarrow 1.0$ )	96.53 ( $\downarrow 0.4$ )	<b>97.0 (<math>\downarrow 0.0</math>)</b>	96.66 ( $\downarrow 0.3$ )	93.4 ( $\downarrow 1.1$ )	94.11 ( $\downarrow 0.4$ )	93.38 ( $\downarrow 1.1$ )
SWIN-T (81.47)	90.64 ( $\downarrow 1.0$ )	90.89 ( $\downarrow 0.7$ )	90.27 ( $\downarrow 1.3$ )	96.61 ( $\uparrow 0.4$ )	96.82 ( $\uparrow 0.6$ )	96.6 ( $\uparrow 0.4$ )	89.66 ( $\downarrow 2.0$ )	90.86 ( $\downarrow 0.8$ )	89.68 ( $\downarrow 1.9$ )
EfficientNetV2-S (84.22)	94.84 ( $\downarrow 0.2$ )	<b>95.13 (<math>\uparrow 0.1</math>)</b>	94.96 ( $\downarrow 0.1$ )	96.22 ( $\downarrow 0.5$ )	96.48 ( $\downarrow 0.2$ )	96.28 ( $\downarrow 0.4$ )	89.18 ( $\downarrow 3.6$ )	92.03 ( $\downarrow 0.8$ )	89.02 ( $\downarrow 3.8$ )
ViT-B-16 (81.07)	86.42 ( $\downarrow 1.0$ )	86.34 ( $\downarrow 1.0$ )	86.54 ( $\downarrow 0.8$ )	96.12 ( $\downarrow 0.7$ )	96.3 ( $\downarrow 0.5$ )	96.25 ( $\downarrow 0.6$ )	86.67 ( $\downarrow 1.5$ )	87.61 ( $\downarrow 0.6$ )	86.94 ( $\downarrow 1.2$ )
ConvNext-S (83.61)	84.56 ( $\downarrow 4.6$ )	87.29 ( $\downarrow 1.9$ )	78.48 ( $\downarrow 10.7$ )	96.3 ( $\downarrow 0.4$ )	96.24 ( $\downarrow 0.5$ )	96.18 ( $\downarrow 0.5$ )	92.15 ( $\downarrow 1.2$ )	92.87 ( $\downarrow 0.5$ )	92.24 ( $\downarrow 1.1$ )

client has a training and validation set, with the local validation set used to determine good local training hyper-parameters. After that, clients train on the union of their two sets, and accuracy is reported on the original, pooled, test dataset of 17,778 images.

The **Abdomen-SSL** dataset was created by extracting 20 slices around the center of each volume in 4 abdominal CT datasets [23, 24, 25], cropping around the subject, resizing to 224x224 and copying the channel over, resulting in  $\sim 21,000$  whole abdomen images. As seen in Fig.1, Abdomen-SSL is quite different to OrganAMNIST. Due to OrganAMNIST’s uniqueness, it is difficult to design a more similar source dataset. However, SSL pre-training can still help the models learn general organ structures and channel redundancy.

**Fed-ISIC** [22] consists of 23,247 RGB skin lesion images with 8 classes, split across 6 clients representing different datacenters and imaging technologies. Fed-ISIC exhibits very high heterogeneity in size and label imbalance, so performance is measured through balanced accuracy, defined as the average recall on each class. We follow the pre-processing in [22], applying color constancy, and centre-cropping while maintaining the aspect ratio.

**Skin-SSL** was created from 3 skin lesion datasets [26, 27, 28], with the largest contributor being ISIC-2020, which has no overlap with Fed-ISIC, and consists predominantly of benign samples.

For all settings, besides federated training, we also train a model on the pooled dataset to compare the FL models against.

### 3.2. Hyper-parameters

In order to concentrate on the ARIAs’ effects, we fix as many factors as possible to reasonable and commonly used values. All networks are trained using the same hyper-parameters using Automatic Mixed Precision (AMP). All random seeds are fixed to the same value for all networks, and results are averaged across two seeds. Training takes  $\sim 1.5$  hours on average per client on an NVIDIA A100 GPU. Our code, which will be made publicly available, is built on NVFlare [29] and can be deployed in a simulated or real federation. For OrganAMNIST training, we use momentum SGD with ( $lr = 0.01$ ,  $m = 0.9$ ) and a cosine annealing schedule, a batch size of 128, and 50 local steps. For Fed-ISIC, we follow [22] and train for 20 rounds, using a batch size of 64 with Adam with  $lr = 5e-4$  and a cosine annealer, but increase the local steps to 200 to allow the biggest client to see all of its data. After examining the client training accuracies, and as a *parity measure* against pre-trained models, when training from scratch we use 600 local steps. Due to the label imbalance, a Weighted Focal Loss with locally computed statistics, as in [22], is used.

## 4. RESULTS AND DISCUSSION

The IID OrganAMNIST experiment (Table 3) serves as a baseline, showing that all architectures, if pre-trained on ImageNet, can virtually solve the task, and achieve very low gaps from the central training scenario when heterogeneity is not an issue. This points to the utility of IN weights, even for IID federated medical datasets. We note that model throughput is not correlated to performance, as DenseNet performs the best while also having the lowest memory footprint. For the heterogeneous tasks (Tables 1, 2), interesting phenomena emerge as discussed in the next paragraphs. More importantly, for Fed-ISIC (Table 1), contrary to the original paper’s claim [22], in our experiments FL not only boosts performance, but on occasion even outperforms central training; this is possible due to the evaluation metric being the average of metrics on separate client validation sets, since the parameter averaging of FL implicitly avoids biasing the model towards the biggest clients at the expense of the smaller ones. This highlights the utility of FL for naturally federated datasets.

### 4.1. The effect of residual network depth, width, and density of connections

Despite deepening and widening generally improving the centrally trained model, the increased central training accuracy was not transferred to FL training. Hence, in our findings, ResNets do not scale well in FL tasks, as ResNet-18 outperforms its deeper and wider counterparts in all settings except for Fed-ISIC with IN weights (Table 1), where the much larger and slower WRN-50-2 is modestly better. If a low memory footprint is a high-priority, we note that increasing the density of residual connections by using a DenseNet-121, which has much fewer parameters than all other networks, performs just as well or better depending on the task, suggesting that its salient characteristic, feature re-use, is beneficial for FL.

### 4.2. The effects of normalization methods

It has been widely discussed, most recently in [13], that BN impedes FL performance under heterogeneous settings due to the local clients calculating statistics that are not representative of each other’s datasets. Simultaneously, BN is reliant on the batch size being sufficiently big to accurately approximate the mean and variance, in contrast to LN and SWS. OrganAMNIST is grayscale and training used a big batch size (128); as a result, we observe (Tables 2, 3) that randomly initialized BN models outperform LN and SWS ones, under both IID and non-IID distributions, but this benefit does not transfer when the models are pre-trained. For the RGB Fed-ISIC,

where the batch size was 64, BN could not help random models as much, and when using IN weights the top three models all use LN or SWS.

When comparing LN and SWS, we note that while LN networks suffer when randomly initialised, the NF-ResNet (which uses SWS) is not as susceptible, even performing the best out of all random models on Fed-ISIC. This makes NF networks and SWS even more promising for FL applications.

Besides normalisation, BN is known to induce a regularization effect. How generalization is affected in FL when substituting BN for LN or SWS remains an open question.

#### 4.3. Are transformers better than convolutional networks?

In general, performance between transformers and convolutional models was very similar with the latter being marginally better when using IN weights. Perhaps due to their data-hungry nature (lack of inductive bias), randomly initialized transformers performed poorly. We also did not find scale to be crucial for this performance, as SWIN-T outperformed the much bigger and slower ViT-B. Moreover, SSL pre-training greatly increases transformer performance specifically, and even outperforms IN weights in Fed-ISIC, despite the lack of longer training and tuning of the SSL pipeline (which would have likely further increased performance). This strengthens the argument for the use of transformer models in medical FL where target domains are usually dissimilar to the natural images of ImageNet, provided suitable datasets to conduct SSL are available.

#### 4.4. Which is the best aggregation strategy?

In OrganAMNIST, FedOpt, on average, increases test accuracy by 0.68% and 2.4% compared to FedAvg for the IID and non-IID case respectively, while the difference between SCAFFOLD and FedAvg is negligible. As FedOpt introduces more hyper-parameters, it is possible that more tuning would further improve results. In Fed-ISIC, FedOpt led, on average, to a loss of 0.59% balanced accuracy, but SCAFFOLD consistently improved performance (1.32% on average), meaning that if the extra memory and bandwidth are not an issue, it is worth considering. This is in-line with its design being for heterogeneous cross-silo, full participation settings, like ours. Despite that, a very important result is that the best ARIA uses FedAvg (Table 1, IN pre-training). Overall, the benefits of switching the architecture are in fact greater than those of switching the aggregation method, suggesting we need to re-examine how far we have progressed since the introduction of FedAvg.

#### 4.5. Does SSL pre-training help?

For the SSL part of our study we forced ourselves to devise SSL datasets & strategies as close as possible to target tasks, mirroring what the medical imaging FL community faces in practice. Skin-SSL pre-training is predictably more useful (Table 1), and greatly increases the performance of all models (especially transformers) vs random initialization. Despite the much shorter pre-training time and lack of extensive SSL tuning compared to IN pre-training, the SSL pre-trained ConvNext-S with SCAFFOLD nearly achieves the best overall performance. While Abdomen-SSL pre-training generally lowered performance, it helped "prime" ConvNext-S and NF-ResNet-50 compared to no-pretraining, indicating it can help counteract the reduction in regularization due to not using BN.

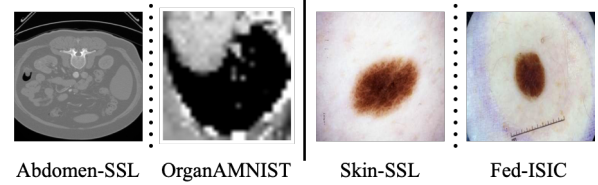


Fig. 1. Samples from the SSL and respective target datasets.

## 5. CONCLUSION

In this work we conduct the first comprehensive study on ARIAs for federated cross-silo visual classification. We attempt to give answers to which architectures and aggregation methods perform the best, provide some new insight into the problems with BN previously discussed in the literature, and into how SSL pre-training can be leveraged in combination with the above to improve performance. Our work can inform practitioners in the (typical for medical imaging) cross-silo setting regarding the ARIAs they employ in real-world scenarios, and motivate researchers to explore further in segmentation and personalized FL tasks.

## 6. COMPLIANCE WITH ETHICAL STANDARDS

IEEE-ISBI supports the standard requirements on the use of animal. This research study was conducted retrospectively using human subject data made available in open access by [21, 22, 23, 24, 25, 26, 27, 28]. Ethical approval was not required as confirmed by the license attached with the open access data.

## 7. ACKNOWLEDGMENTS

The authors have no relevant interests to disclose.

## 8. REFERENCES

- [1] Micah J Sheller, Brandon Edwards, G Anthony Reina, Jason Martin, Sarthak Pati, Aikaterini Kotrotsou, Mikhail Milchenko, Weilin Xu, Daniel Marcus, Rivka R Colen, et al., "Federated learning in medicine: facilitating multi-institutional collaborations without sharing patient data," *Scientific reports*, vol. 10, no. 1, pp. 12598, 2020.
- [2] Brendan McMahan, Eider Moore, Daniel Ramage, Seth Hampson, and Blaise Aguera y Arcas, "Communication-efficient learning of deep networks from decentralized data," in *Artificial intelligence and statistics*. PMLR, 2017, pp. 1273–1282.
- [3] Tzu-Ming Harry Hsu, Hang Qi, and Matthew Brown, "Measuring the effects of non-identical data distribution for federated visual classification," *arXiv preprint arXiv:1909.06335*, 2019.
- [4] Sai Praneeth Karimireddy, Satyen Kale, Mehryar Mohri, Sashank Reddi, Sebastian Stich, and Ananda Theertha Suresh, "Scaffold: Stochastic controlled averaging for federated learning," in *International conference on machine learning*. PMLR, 2020, pp. 5132–5143.
- [5] Sara Pieri, Jose Renato Restom, Samuel Horváth, and Hisham Cholakkal, "Handling data heterogeneity via architectural design for federated visual recognition," in *Thirty-seventh Conference on Neural Information Processing Systems*, 2023.

- [6] Hong-You Chen, Cheng-Hao Tu, Ziwei Li, Han Wei Shen, and Wei-Lun Chao, "On the importance and applicability of pre-training for federated learning," in *The Eleventh International Conference on Learning Representations*, 2022.
- [7] John Nguyen, Jianyu Wang, Kshitiz Malik, Maziar Sanjabi, and Michael Rabbat, "Where to begin? on the impact of pre-training and initialization in federated learning," *arXiv preprint arXiv:2210.08090*, 2022.
- [8] Liangqiong Qu, Yuyin Zhou, Paul Pu Liang, Yingda Xia, Feifei Wang, Ehsan Adeli, Li Fei-Fei, and Daniel Rubin, "Rethinking architecture design for tackling data heterogeneity in federated learning," in *Proceedings of the IEEE/CVF Conference on Computer Vision and Pattern Recognition*, 2022, pp. 10061–10071.
- [9] Micah Goldblum, Hossein Souri, Renkun Ni, Manli Shu, Viraj Prabhu, Gowthami Somepalli, Prithvijit Chattopadhyay, Mark Ibrahim, Adrien Bardes, Judy Hoffman, et al., "Battle of the backbones: A large-scale comparison of pre-trained models across computer vision tasks," *arXiv preprint arXiv:2310.19909*, 2023.
- [10] Kaiming He, Xiangyu Zhang, Shaoqing Ren, and Jian Sun, "Identity mappings in deep residual networks," in *Computer Vision—ECCV 2016: 14th European Conference, Amsterdam, The Netherlands, October 11–14, 2016, Proceedings, Part IV 14*. Springer, 2016, pp. 630–645.
- [11] Sergey Zagoruyko and Nikos Komodakis, "Wide residual networks," *arXiv preprint arXiv:1605.07146*, 2016.
- [12] Gao Huang, Zhuang Liu, Laurens Van Der Maaten, and Kilian Q Weinberger, "Densely connected convolutional networks," in *Proceedings of the IEEE conference on computer vision and pattern recognition*, 2017, pp. 4700–4708.
- [13] Jike Zhong, Hong-You Chen, and Wei-Lun Chao, "Making batch normalization great in federated deep learning," *arXiv preprint arXiv:2303.06530*, 2023.
- [14] Andrew Brock, Soham De, and Samuel L Smith, "Characterizing signal propagation to close the performance gap in unnormalized resnets," *arXiv preprint arXiv:2101.08692*, 2021.
- [15] Alexey Dosovitskiy, Lucas Beyer, Alexander Kolesnikov, Dirk Weissenborn, Xiaohua Zhai, Thomas Unterthiner, Mostafa Dehghani, Matthias Minderer, Georg Heigold, Sylvain Gelly, et al., "An image is worth 16x16 words: Transformers for image recognition at scale," *arXiv preprint arXiv:2010.11929*, 2020.
- [16] Ze Liu, Yutong Lin, Yue Cao, Han Hu, Yixuan Wei, Zheng Zhang, Stephen Lin, and Baining Guo, "Swin transformer: Hierarchical vision transformer using shifted windows," in *Proceedings of the IEEE/CVF international conference on computer vision*, 2021, pp. 10012–10022.
- [17] Mingxing Tan and Quoc Le, "Efficientnetv2: Smaller models and faster training," in *International conference on machine learning*. PMLR, 2021, pp. 10096–10106.
- [18] Zhuang Liu, Hanzi Mao, Chao-Yuan Wu, Christoph Feichtenhofer, Trevor Darrell, and Saining Xie, "A convnet for the 2020s," in *Proceedings of the IEEE/CVF conference on computer vision and pattern recognition*, 2022, pp. 11976–11986.
- [19] Mathilde Caron, Hugo Touvron, Ishan Misra, Hervé Jégou, Julien Mairal, Piotr Bojanowski, and Armand Joulin, "Emerging properties in self-supervised vision transformers," in *Proceedings of the IEEE/CVF international conference on computer vision*, 2021, pp. 9650–9660.
- [20] Sashank Reddi, Zachary Charles, Manzil Zaheer, Zachary Garrett, Keith Rush, Jakub Konečný, Sanjiv Kumar, and H Brendan McMahan, "Adaptive federated optimization," *arXiv preprint arXiv:2003.00295*, 2020.
- [21] Jiancheng Yang, Rui Shi, Donglai Wei, Zequan Liu, Lin Zhao, Bilian Ke, Hanspeter Pfister, and Bingbing Ni, "Medmnist v2—a large-scale lightweight benchmark for 2d and 3d biomedical image classification," *Scientific Data*, vol. 10, no. 1, pp. 41, 2023.
- [22] Jean Ogier du Terrail, Samy-Safwan Ayed, Edwige Cyffers, Felix Grimberg, Chaoyang He, Regis Loeb, Paul Mangold, Tanguy Marchand, Othmane Marfoq, Erum Mushtaq, et al., "Flamby: Datasets and benchmarks for cross-silo federated learning in realistic healthcare settings," *Advances in Neural Information Processing Systems*, vol. 35, pp. 5315–5334, 2022.
- [23] Holger R Roth, Le Lu, Amal Farag, Hoo-Chang Shin, Jiamin Liu, Evrim B Turkbey, and Ronald M Summers, "Deeporgan: Multi-level deep convolutional networks for automated pancreas segmentation," in *Medical Image Computing and Computer-Assisted Intervention—MICCAI 2015: 18th International Conference, Munich, Germany, October 5–9, 2015, Proceedings, Part I 18*. Springer, 2015, pp. 556–564.
- [24] Nicholas Heller, Fabian Isensee, Dasha Trofimova, Resha Tejpaul, Zhongchen Zhao, Huai Chen, Lisheng Wang, Alex Golts, Daniel Khapun, Daniel Shats, et al., "The kits21 challenge: Automatic segmentation of kidneys, renal tumors, and renal cysts in corticomedullary-phase ct," *arXiv preprint arXiv:2307.01984*, 2023.
- [25] Amber L Simpson, Michela Antonelli, Spyridon Bakas, Michel Bilello, Keyvan Farahani, Bram Van Ginneken, Annette Kopp-Schneider, Bennett A Landman, Geert Litjens, Bjørn Menze, et al., "A large annotated medical image dataset for the development and evaluation of segmentation algorithms," *arXiv preprint arXiv:1902.09063*, 2019.
- [26] Jeremy Kawahara, Sara Daneshvar, Giuseppe Argenziano, and Ghassan Hamarneh, "Seven-point checklist and skin lesion classification using multitask multimodal neural nets," *IEEE journal of biomedical and health informatics*, vol. 23, no. 2, pp. 538–546, 2018.
- [27] Andre GC Pacheco, Gustavo R Lima, Amanda S Salomao, Breno Krohling, Igor P Biral, Gabriel G de Angelo, Fábio CR Alves Jr, José GM Esgario, Alana C Simora, Pedro BC Castro, et al., "Pad-ufes-20: A skin lesion dataset composed of patient data and clinical images collected from smartphones," *Data in brief*, vol. 32, pp. 106221, 2020.
- [28] Veronica Rotemberg, Nicholas Kurtansky, Brigid Betz-Stablein, Liam Caffery, Emmanouil Chousakos, Noel Codella, Marc Combalia, Stephen Dusza, Pascale Guitera, David Gutman, et al., "A patient-centric dataset of images and metadata for identifying melanomas using clinical context," *Scientific data*, vol. 8, no. 1, pp. 34, 2021.
- [29] Holger R Roth, Yan Cheng, Yuhong Wen, Isaac Yang, Ziyue Xu, Yuan-Ting Hsieh, Kristopher Kersten, Ahmed Harouni, Can Zhao, Kevin Lu, et al., "Nvidia flare: Federated learning from simulation to real-world," *arXiv preprint arXiv:2210.13291*, 2022.